ADVANCED FUNCTIONAL MATERIALS
www.afm-journal.de

Demonstrating kHz Frequency Actuation for Conducting Polymer Microactuators

Ali Maziz, Cedric Plesse, Caroline Soyer, Claude Chevrot, Dominique Teyssié, Eric Cattan, and Frederic Vidal*

This paper reports results on ionic EAP micromuscles converting electrical into micromechanical response in open-air. Translation of small ion motion into large deformation in bending microactuator and its amplification by fundamental resonant frequency are used as tools to demonstrate that small ion vibrations can still occur at frequency as high as 1000 Hz in electrochemical devices. These results are achieved through the microfabrication of ultrathin conducting polymer microactuators. First, the synthesis of robust interpenetrating polymer networks (IPNs) is combined with a spincoating technique in order to tune and drastically reduce the thickness of conducting IPN microactuators using a so-called "trilayer" configuration. Patterning of electroactive materials as thin as 6 µm is demonstrated with existing technologies, such as standard photolithography and dry etching. Electrochemomechanical characterizations of the micrometer sized beams are presented and compared to existing model. Moreover, thanks to downscaling, large displacements under low voltage stimulation (±4 V) are reported at a frequency as high as 930 Hz corresponding to the fundamental eigenfrequency of the microbeam. Finally, conducting IPN microactuators are then presenting unprecedented combination of softness, low driving voltage, large displacement, and fast response speed, which are the keys for further development to develop new MEMS.

1. Introduction

Electronic conducting polymers (ECP) are reactive materials under a flow of electric current.[1,2] An electrical energy input induces electrochemical reactions, driving several modifications of properties, including volume changes, among others. Indeed, when the ECP is oxidized or reduced electrochemically, ions and solvent molecules are inserted or expelled from the ECP in order to insure the overall electroneutrality and result in a variation of the ECP volume. This behavior makes them particularly interesting in the family of electroactive polymers (EAPs) for actuator applications.[3] Considering that they are lightweight, noiseless, low voltage driven, biocompatible, downsizable and can present large deformations, they are very promising candidates as microactuators in MicroElectro-Mechanical Systems (MEMS). Small scale EAP actuators are potential candidates in numerous applications, including the micromanipulation of living cells, bioanalytical nanosystems, data storage, lab-on-a-chip, microvalve, microswitch, microshutter, cantilever light modulators, microoptical instrumentation, artificial muscles for macro/microrobotics, and so on.[4–6] The microfabrication of ECPs has been extensively demonstrated by Jager,[5,7] Smela[8] and Otero,[9] in which bending bilayer microactuators have been described. However, these materials require immersion in a liquid electrolyte as a source of ions for actuation. Recently, new actuator systems operating in air have been developed and shaped as trilayer devices,[10,11] in which the presence of two electroactive electrodes and a solid polymer electrolyte (SPE) acting as an ion reservoir to draw ions from, is essential.

In those systems, the diffusion phenomena of ions and solvents into the ECP is a rate-limiting step in the actuation performances as with every ionic EAP,[3] making them considered to be slow devices, typically in the range of 1 Hz. In order to increase speed, the ionic conductivity has to be increased and/or the distance between electroactive layers has to be reduced.[12,13] Then the SPE layer plays a key role in the ultimate performances of these electrochemomechanical devices and is the main limiting factor hindering further miniaturization of the conducting polymer actuators operating in air. Indeed, they have to provide suitable elastic modulus, ultimate tensile strength and strechability to reduce the devices' thickness while keeping ionic conductivity as high as possible.

In this field, interpenetrating polymer networks (IPNs) represent an interesting architecture. They are described as the combination of two or more cross-linked polymers synthesized in the presence of one another. By thoughtfully selecting partners for networks, it's possible to combine the ionic conduction properties of the first partner with the rubbery

Dr. A. Maziz, Dr. C. Plesse, Prof. C. Chevrot, Prof. D. Teyssié, Prof. F. Vidal
LPPI – EA2528
Institut des Materiaux
5 mail Gay Lussac, Neuville sur Oise,
Cergy-Pontoise cedex 95031, France
E-mail: cedric.plesse@u-cergy.fr
Dr. C. Soyer, Prof. E. Cattan
IEMN, UMR-8520, Université de Valenciennes, Le Mont Houy
Valenciennes cedex 9 59313, France

DOI: 10.1002/adfm.201400373

properties of the second one, if controlling synthesis leads to a co-continuous phase morphology.[14] In previous works, we reported the synthesis of a 12 µm thin IPN layer by using a hot pressing method combining a polytetrahydrofurane network for mechanical resistance and a poly(ethylene oxide) (PEO) as a solid polymer electrolyte. After interpenetration of two poly(3,4-ethylenedioxythiophene) (PEDOT) electrodes in both faces of the SPE film and swelling in an ionic liquid, a pseudo-trilayer configuration have been obtained leading to 20 µm thick conducting IPN actuator[11] which move with large displacement at a fundamental eigenfrequency of 125 Hz. Patterning of these materials has been performed using photolithography and reactive ion etching (RIE) and freestanding micro-beam actuators (900 µm × 300 µm × 20 µm) have been obtained.[15]

Downscaling open-air actuator thickness below 20 µm has never been done before and is not easy in matter, but it should lead to a drastic increase of system response speed. The relevant scope of this work deals with the synthesis of ultrathin conducting IPN microactuators using the spincoating method and patterning through microsystem techniques. The SPE is synthesized as an IPN based on a PEO network for ionic conductivity with improvement of strain at break by the interpenetration of a high molecular mass elastomer, nitrile butadiene rubber (NBR), within the PEO network. Robust SPE has been obtained with tunable thickness from 30 µm to 600 nm. Ultrathin conducting IPNs were then synthesized by incorporating PEDOT electrodes in both faces of the SPE. Furthermore, the patterning of such trilayer devices through microsystems techniques was demonstrated. The resulting micro-beam actuators were then characterized in terms of free displacement and blocking force. Moreover mechanical responses at unprecedented response speed demonstrate that "so called" ionic actuators are capable of kHz frequency actuation.

2. Results and Discussion

2.1. Synthesis of Ultrathin Solid Polymer Electrolytes

The stumbling block in the development of ultrathin microactuators is the synthesis of ultrathin SPE. While high ionic conductivity in the presence of an electrolyte is the main characteristic required for SPE, the use of materials with rubber like behaviour becomes critical as soon as electrochemomechanical devices are concerned. It has been demonstrated previously that an interpenetrating polymer network architecture can be a powerful approach for such materials, since a co-continuous morphology can combine the specific properties of each polymeric network in a stable manner, for instance: ionic conductivity of the PEO network and mechanical robustness of the rubbery network X in PEO/X IPNs.[16,17] In particular, PEO/NBR IPNs are interesting candidates.[18] Typically, PEO/NBR 50/50 (w/w) IPNs were obtained following an in-situ pathway with sequential polymerization. All the IPN precursors are solubilized in cyclohexanone, a high boiling point solvent. The PEO network was obtained first at 50 °C by free radical copolymerization of poly(ethylene glycol)methyl ether methacrylate (PEGM), as monomer, and poly(ethyleneglycol)dimethacrylate (PEGDM), acting as crosslinker, initiated by dicyclohexylperoxydicarbonate

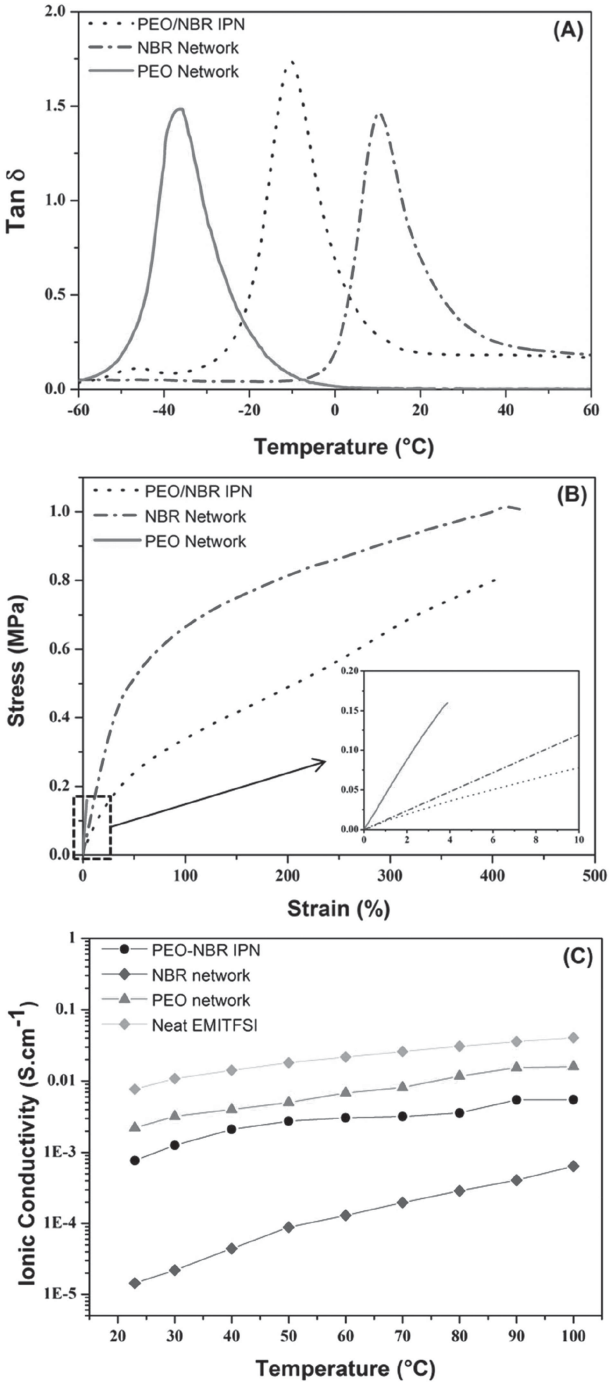

Figure 1. (Thermo)mechanical and ionic conduction properties of 250 µm thick 50/50 PEO/NBR IPN and corresponding single networks. A) tanδ versus temperature, B) stress versus strain, and C) ionic conductivity as a function of temperature. The ionic conductivity of pure EMITFSI is reported for comparison.

(DCPD). Raising the temperature to 160 °C, NBR was then cross-linked in the presence of the PEO network by DCP. Thick films (250 µm) were first prepared in glass molds in order to perform thermomechanical and ionic conduction characterizations. **Figure 1**A presents the typical viscoelastic behavior of the 250 µm thick IPN and corresponding single networks.

The PEO/NBR IPN presents two tanδ peaks. The tanδ peak with the lowest intensity is observed at –45 °C. It can be assigned to the viscoelastic response of a PEO-rich phase, since its relaxation temperature is close (ΔT = 9 °C) to that of the PEO single network. However, the magnitude of the tanδ peak is very small compared to the weight ratio of the PEO partner in the IPN (50%) indicating that the amount of PEO phase-separated domains is probably very limited. More interestingly, the main IPN response is characterized by only one major α relaxation occurring at –10 °C, a temperature situated between those of the PEO and NBR single networks, –35 °C and 20 °C respectively. Besides the small relaxation at –45 °C, the mechanical signature of each partner does not appear anymore and the IPN almost appears as a homogenous material at the DMA scale. This kind of viscoelastic behavior has been described for the IPN architecture by Sperling et al.[14] It is usually assigned to an interpenetration degree of the two partners at a molecular level. This interpenetrated structure, as well as the relative content of each partner (50/50) should lead to a phase co-continuity across all the bulk and provide a combination of properties.

Tensile stress measurements are depicted in Figure 1B. PEO single network have a weak elongation at break of 4% for a stress of 0.15 MPa. The Young's modulus, obtained from the initial slope, is 4.2 MPa. This poor mechanical resistance of the PEO indicates that such a single network is too brittle as SPE for an actuator application. On the other hand, NBR single network presents a Young's modulus of 1.2 MPa and breaks at 430% strain for a stress of 1 MPa which makes this elastomer very interesting for the intended application. However, NBR network is useless since it demonstrates low ionic conductivity in the presence of EMITFSI.[19,20] The Young's modulus of the PEO/NBR IPN is 0.69 MPa, which is lower than that of both single networks. In other words, the mechanical response is not a mean value of the two partners. This behavior is consistent with the viscoelastic behavior of the IPN where the α relaxation can correspond to the NBR phase plasticized by the PEO chains. Elongation and stress at break of around 400% and 0.8 MPa respectively are achieved, demonstrating that the mechanical properties are mainly ruled by the rubbery properties of NBR, besides it contains 50% of brittle PEO network.

Figure 1C shows the temperature dependence of ionic conductivity of the PEO and NBR single networks swollen with 1-ethyl-3methylimidazolium bis(trifluoromethylsulfonyl)imide (EMITFSI). As expected, it demonstrates that the PEO partner is much more conductive than the NBR one (more than two orders of magnitude at room temperature). For EMITFSI swollen IPN, conductivity values are just slightly lower than that of PEO single networks. At room temperature, IPNs and PEO single networks have almost the same ionic conductivity, 1.5×10^{-3} S cm^{-1} and 3×10^{-3} S cm^{-1} at 25 °C, respectively. Therefore, the presence of 50% of a poorly conductive NBR within the PEO does not significantly impact the IPN ionic conductivity. The combination of rubber like behaviour and ionic conductivity makes this PEO/NBR IPN a promising candidate as an ultrathin and robust SPE.

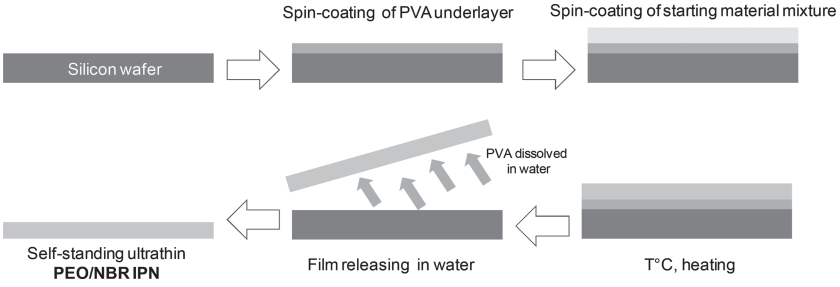

Figure 2. Approach used to develop a ultrathin PEO/NBR IPNs.

Next, the decrease of IPN thickness was performed by spin-coating. Spin-coating is a well-known method for obtaining thin films on substrates, with the final thickness depending, among other things, on the solution viscosity and the spinner speed. Very few works deal with (semi-)IPN synthesis as thin films using this approach.[21,22] Moreover, the resulting materials are usually only used as substrate coatings. Recently, spin-coating and lift-off synthesis of 32µm PVdF membrane[13] and even 500 µm semi-IPN[23] for actuator purposes have been described. **Figure 2** describes the general procedure for obtaining ultrathin PEO/NBR films. The reactive mixture is applied by spin-coating on a Si wafer coated with a polyvinylalcohol (PVA) underlayer, and the resulting thin viscous layer is thermally cured under inert atmosphere. After solubilization of the PVA underlayer in water, the IPNs are released as thin membranes that can be manipulated without suffering from cracking.

Depending on the spin speed PEO/NBR solid polymer electrolytes are obtained with tunable thicknesses from 30 µm (1000 rpm/1000 rpm s^{-1} for 30 s) to 0.6 µm (9000 rpm/8000 rpm s^{-1} for 30 s) with very good reproducibility (see Supporting Information).

2.2. Synthesis of Ultrathin Conducting IPNs

Three SPE thicknesses (3.5, 8 and 14 µm) were chosen for the synthesis of three conducting IPNs. The EDOT monomer was carefully incorporated into the ultrathin IPNs by gas-phase swelling under reduced pressure, until the swelling ratio reached an optimized value of 120%. Next, samples were dipped into an aqueous $FeCl_3$ solution at 40 °C for the oxidative chemical polymerization of EDOT. The polymerization time was set according to the IPN thickness, 10, 15 and 20 min respectively. The pseudo trilayer morphology of the resulting conducting IPNs was confirmed by EDS spectroscopy with a sulfur mapping across the thickness, since sulfur atoms can be considered as the chemical signature of PEDOT. **Figure 3** clearly shows a non-homogeneous distribution of PEDOT throughout the thickness of the film. PEDOT layers are then interpenetrated in the SPEs as two separate and parallel electrodes and mimic a trilayer configuration.

The estimated electronic conductivity of the conducting layers is reported in **Table 1**. The PEDOT layer conductivity decreases from 73 S cm^{-1} for the thinnest layer to 36 S cm^{-1}

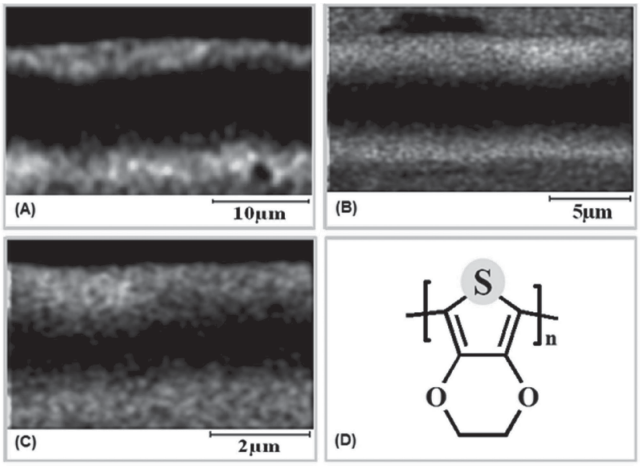

Figure 3. EDS pictures with sulfur atom cartography (yellow dots) of the three non-swollen conducting IPN with a thickness of A) 14 µm, B) 8 µm, and C) 3.5 µm. D) PEDOT structure.

for the thickest one. This case illustrates the phenomenon occurring in chemical synthesis of electrically conductive polymers. The conductivity shows a maximum for short polymerization time and decreases gradually with time. Indeed, structural changes may take place in the polymer backbone that lead to the lowering of the conjugation length and hence to the decrease of electrical conductivity, as observed in the case of polypyrrole.[24]

2.3. Patterning of Conducting IPNs

Patterning of conducting IPNs was performed with the help of photolithography and dry etching[11] as summarized in **Figure 4**A. After lift-off of the patterned conducting IPN, the micro-beams were immersed in neat EMITFSI for 72 hours to obtain a microactuator active in the open air. A small increase in the total thickness of the samples was observed during swelling leading to 6, 12, and 19 µm thick films respectively.

As illustrated on SEM images (Figures 4B,D,F) microfabrication of conducting IPN microactuators can be performed with precise control of the geometry for the three different thicknesses. An isotropic etching was confirmed with a detailed observation of the microbeam walls and the free end. Indeed, while quasi-vertical sidewalls were obtained for the thinnest beam (Figure 4C), etching isotropy was more and more pronounced as the total thickness of the samples is increased (Figures 4E,G), that is, as the required etching time is increased. This result is consistent with a chemical etching of the beam in the CF_4/O_2 plasma leading to an etching of the sides of the microbeam, especially in the case of samples with high thickness. For the subsequent electrochemomechanical

Table 1. Characteristics of the three different conducting IPNs.

Dry conducting IPN thickness [µm]	EMITFSI swollen Conducting IPN thickness h [µm]	PEDOT electrode thickness h_1 [µm]	PEDOT content [%wt]	Electronic Conductivity [S cm^{-1}]
3.5	6	1.3	19.7	73± 10
8	12	2.2	17.5	62±5
14.5	19	3.0	15.9	36±7

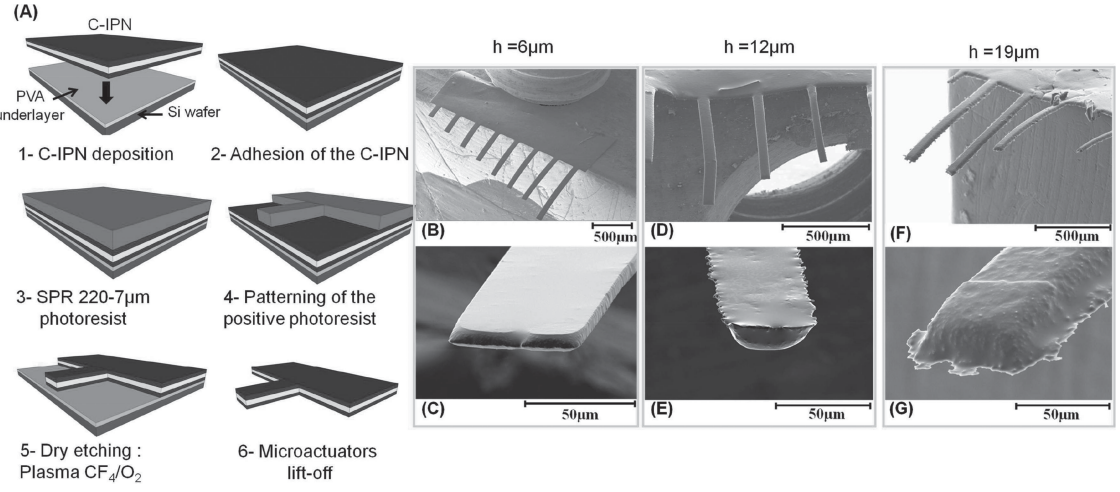

Figure 4. A) general procedure for the conducting IPN patterning using photolithography and dry etching. B,D,F) SEM images of microactuators after batch microfabrication for 6, 12, and 19 µm respectively. C,E,G) magnification of the microbeam free end highlighting the isotropic etching for 6, 12, and 19 µm respectively.

characterizations microactuators with the same length (690 µm) and same width (45 µm) have been fabricated.

2.4. Microactuator Characterizations

The influence of the thickness on electromechanical responses of the synthesized microactuators has been characterized through their limit performances, that is, the strain difference corresponding to the maximum displacement and the blocking force. The strain difference is reported on **Figure 5**A.

Interestingly, the actuator deformation remains almost constant (90% of the initial amplitude at low frequency) up to 20, 5, and 5 Hz respectively with the microactuator thicknesses indicating that full actuation is available up to this frequency. Since the actuation is mainly ruled by the redox process in the conducting polymer actuators,[2] it can be concluded that complete oxidation/reduction of the conducting polymer electrodes occurs. Then the synthesis of ultrathin SPE allows a drastic decrease of diffusion distances and then promotes fast actuation speed. The maximum strain difference at 1 Hz is equal to 0.2, 0.55, and 0.9% for the 6, 12, and 19 µm thick actuators

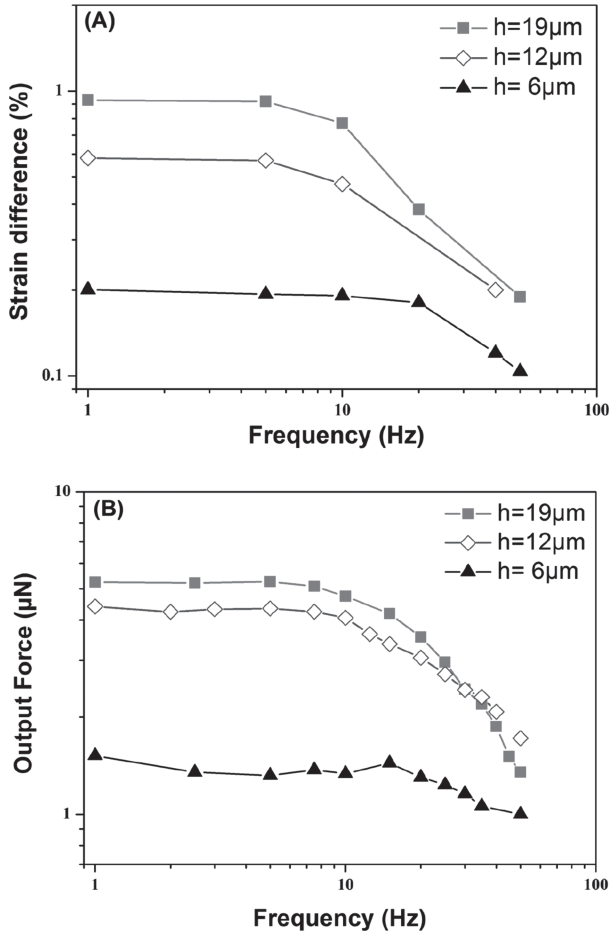

Figure 5. A) strain difference as a function of frequency of the three microactuators ($L \times w$: 690 µm × 45 µm) under ±2 V square wave potential. B) output force as a function of the frequency for the three microactuators ($L \times w$: 690 µm × 45 µm) under ±2 V square wave potential.

corresponding to a peak-to-peak displacement of 121, 178, and 180 µm. These results mean that the thinnest sample shows the lowest PEDOT strain. This result can be explained by the presence of some short circuits between the PEDOT electrodes through the thickness of the materials which is even more pronounced for the thinnest one. This highlights that precise control of the ECP interpenetration is a key to obtain actuation, but also that an SPE thickness of 3.5 µm may be close to the thickness limit for conducting IPN obtained by oxidative polymerization of EDOT. For higher frequencies, the strain difference decreases indicating that less and less PEDOT is undergoing a redox process and this trend is more pronounced as the actuator thickness increases.

Figure 5B presents output force as a function of the frequency under ±2 V square wave potential for the three different samples. A behavior similar to that of free strain difference is observed. First the blocking force remains almost constant (90%) from low frequency to 20, 12.5, and 10 Hz respectively for the three different thicknesses. Once again, this result indicates that the electrochemomechanical process is fast enough to fully occur up to such frequency. It is noteworthy to mention that for most of the ECP based actuators reported in the literature,[3,25,26] the actuation performances decrease sharply after 1 Hz applied frequency. In this study, it is clearly demonstrated the benefit of downscaling the microactuators thickness in order to increase the operating speed.

As depicted, the maximum output force at low frequency increases with the sample thickness from 1.5 to 5.2 µN respectively. These experimental values have been compared with predictions of mechanical models developed for trilayer actuators.[27,28] Typically Madden and Alici state that Equation (1) relates output force, deformation and device characteristics:

$$\frac{1}{R}EI + \varepsilon_0 E_1 w h_1 (h_1 + h_2) - FL = 0 \quad (1)$$

where $EI = E_1 I_1 + E_2 I_2$ is the flexural rigidity of the whole actuator (E_x and Ix designing the Young's Modulus and the inertial moment of the layers with 1 and 2 for the ECP layer and SPE layer respectively), w is the width, ε_0 is the free strain in the ECP layer which is described as a function of the strain to charge ratio and the charge density, h_1 and h_2 are the thicknesses of the ECP and SPE layer respectively and L is the length.

Equation (1) predicts the two limit performances of the actuator:

Maximum displacement at the actuator tip: (i.e., $F = 0$).

$$\varepsilon_0 = -\frac{EI}{R E_1 w h_1 (h_1 + h_2)} \quad (2)$$

Blocking force assuming the radius of curvature is extremely large ($1/R \approx 0$).

$$F = \frac{E_1 w \varepsilon_0 h_1 (h_1 + h_2)}{L} \quad (3)$$

The first case is used to determine the value of ε_0, provided that the radius of curvature R, and the numerical values of the other parameters in Equation (2) are known. The radius of

curvature is measured from the actuator strain difference as given at low frequency in Figure 5A. Assuming that the thickness of the interpenetrated PEDOT electrodes remain constant during swelling of the actuator in EMITFSI,[26] that is, the interpenetrated PEDOT layers are hardly swollen, the values of h_1 are those reported in Table 1 and the SPE thickness h_2 is equal to 3.4, 7.6, and 13 µm for the 6, 12, and 19 µm EMITFSI swollen conducting IPNs respectively.

While the Young's modulus E_2 of the SPE is equal to 0.69 MPa, the Young's modulus E of the actuator can be calculated using Hooke's law (see Supporting Information). The experimental stiffness k for the 12 µm beam is equal to 14.5 ± 0.7 mN m^{-1} at 690 µm from the clamped beam. According to Equation (4) the Young's modulus E of the microbeam can be calculated and is equal to 291 ± 15 MPa.

$$E = \frac{12kL^3}{3wh^3} \tag{4}$$

Knowing the dimensions of each layer and their inertial moment,[27] the Young's Modulus E_1 of the PEDOT interpenetrated layer can be calculated from the expression of EI and is equal to 328 ± 50 MPa. From Table 1 it can be observed that the PEDOT content is decreasing (19.7, 17.5, and 15.9%) when the thickness of the conducting IPN is increasing from 6 to 19 µm. Interestingly we can notice that the PEDOT vs. conducting IPN volume ratio ($2h_1/h$) is decreasing also (43.3, 36.7, and 31.7%) in the same proportions when the thickness is increasing. Then the PEDOT volume ratio on PEDOT content remains constant (2.09 ± 0.1) and indicates that the conducting electrodes present the same average local concentration of PEDOT for the three considered conducting IPNs. As a consequence we can assume in the subsequent calculations that the ECP electrodes must present the same Young's modulus E_1in the three samples.

The ε_0 values are then calculated and employed to estimate the force produced by the actuator as described by Equation (3).

As demonstrated on **Figure 6** the calculated output forces predict the trend and the order of magnitude of the experimental values (~µN) for the three microactuators. However accuracy of the prediction is not fully satisfactory. It appears that even if there is some uncertainty on parameters numerical values the proposed model was developed for classical trilayer actuators. In the case of conducting IPNs the interpenetrated nature of PEDOT may lead to a gradient of properties through the thickness of the samples. For instance, a gradient of the Young's modulus as well as a non-constant value of the strain-to-charge ratio and the charge density inside the electrodes probably have to be taken into account. This means that the non-homogenous nature of each layer requires a specific model for conducting IPN actuators to be developed and is under investigation.

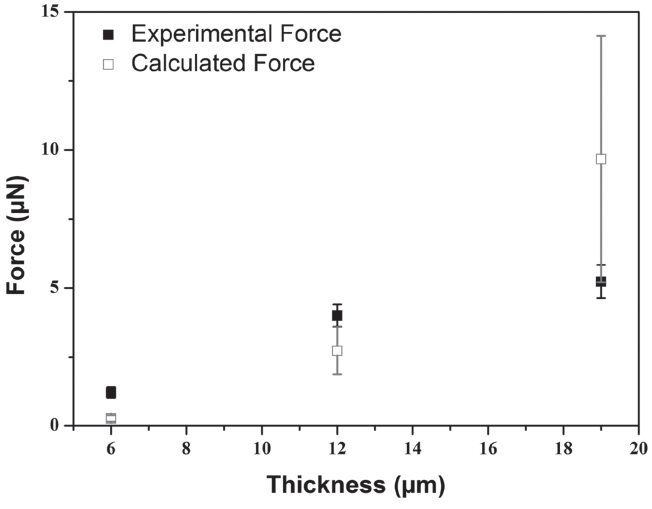

Figure 6. Experimental (■) and calculated (□) output forces at 1Hz as a function of the sample total thickness.

2.5. Resonant Frequency

The decrease in thickness of these actuators achieved fast responses during the actuation test. It will now be interesting to study if a high resonant frequency can be observed for such systems. The resonant frequency, in Hertz, and subsequent harmonics for a cantilever beam can be calculated according to:[29]

$$f_n = \frac{1}{2\pi\sqrt{12}}\alpha_n \frac{h}{L^2}\sqrt{\frac{E}{\rho}} \tag{5}$$

Where α_n is the resonant frequency mode (1.875 for fundamental resonant frequency) and ρ is the volumetric mass density.

From this equation it appears that the resonant frequency is directly proportional to the thickness h and increases as the inverse of the square of the length L. Then, patterning of thin microactuators with small length should lead to beams with high fundamental resonance frequency.

Since the Young's modulus of the 12 µm beam is 291 ± 15 MPa, and taking into account that the average volumetric mass density of the material is equal to 1.7 $g.cm^{-3}$, the fundamental resonant frequency of the 690 µm × 45 µm × 12 µm microactuator should occur at 900 ± 20 Hz, a value far above the response speed of previously described fast ECP actuators.[12,30] The **Figure 7** presents the strain difference as a function of the electrical stimulation frequency. The potential window was here increased to ±4 V in order to increase speed of ionic motion in the membrane. Indeed, as described previously,[12,30–32] an increase in the applied potential may increase the actuation rate. However, no measurement are performed below 50 Hz to limit the degradation of the PEDOT electrodes that may occur under high potential for long periods of time.[31]

At 50 Hz the strain difference is equal to 0.5%, which is almost the same as the value obtained below 10 Hz for ±2 V square wave potential (Figure 5(A)), demonstrating the impact of the enlargement of the potential window. This result indicates that almost complete actuation, and then redox process, may take place at such a high frequency. Above 50 Hz, the strain difference is decreasing, corresponding to a decrease of the redox reaction contribution. At 500 Hz, the microactuator still presents a small strain difference of 0.2%. While it is difficult to conclude about the share of the redox process in the actuation response at this rate, it can be supposed that mainly small movements of ions are

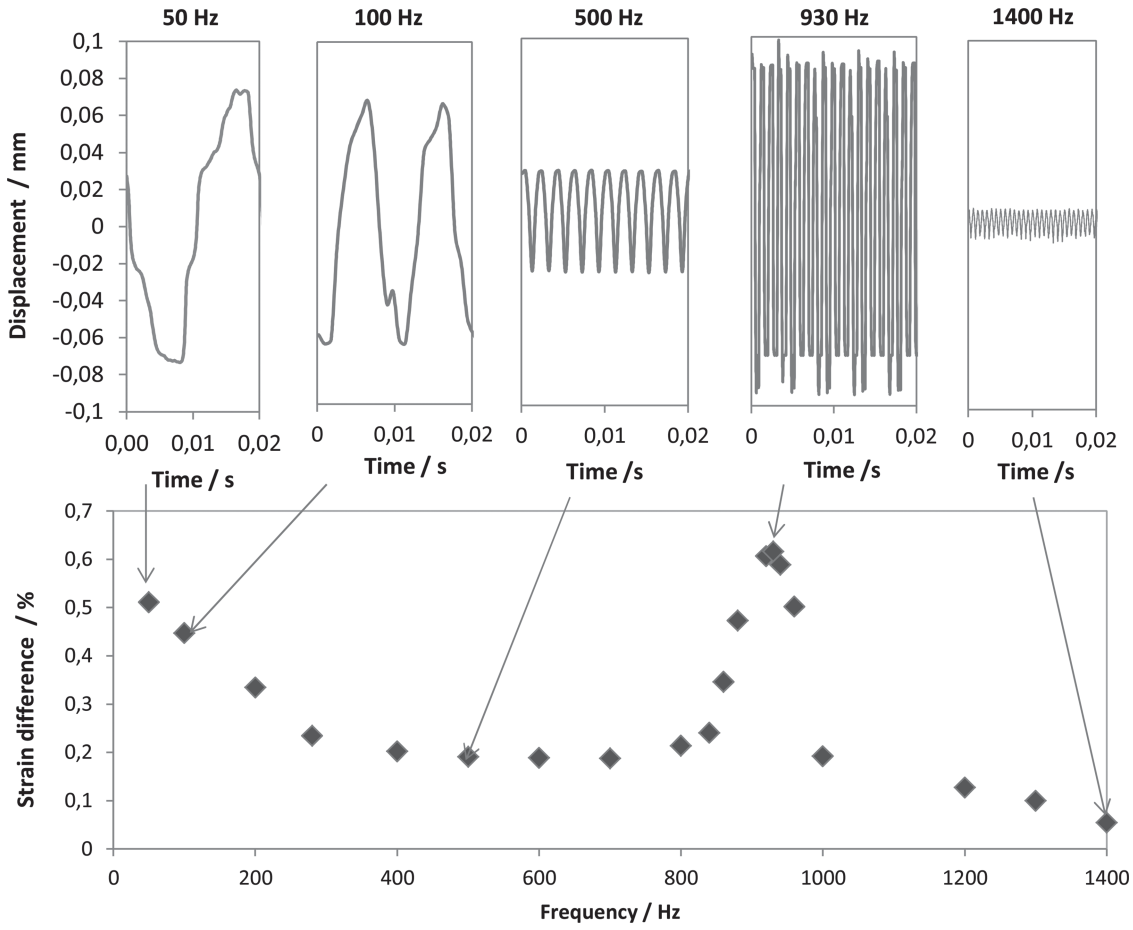

Figure 7. Free strain as a function of frequency of the microactuator ($L \times w \times h$: 690 µm × 45 µm × 12 µm) under ±4 V square wave potential. Insets: tip displacement versus time at 50, 100, 500, 930, and 1400 Hz.

still involved in actuation at such frequency. However, even small ion movements seem to be sufficient to promote oscillatory bending of the microbeam. Interestingly, when the frequency reaches 930 Hz, a large strain is measured with a peak-to-peak displacement 190 µm at 690 µm of the clamped beam.

This frequency is close to the theoretical calculated value of the fundamental resonant frequency and can be associated with mechanical amplification of small electrically induced strain. Finally, the remaining small vibration of the beam at 1400 Hz can be evidence again that small vibrations of ionic species still exist at such a rate. Patterning of these materials into microbeams with controlled lengths could be performed in order to control the value of the resonant frequency. These materials present then unique combination of properties when compared to conventional electrostatic and piezoelectric microactuators at similar length scales[33] since they combine high response speed, large deformation under low voltage, and low temperature patterning process compatible with soft substrate.

3. Conclusion

We have demonstrated the synthesis of ultrathin conducting IPNs by spin-coating techniques. The interpenetrated NBR network provided sufficient mechanical properties to handle materials as thin as 3.5 µm without impairing the ionic conductivity brought by the PEO partner. PEDOT was successfully interpenetrated on the both sides of the film with three different thicknesses, mimicking trilayer architecture. Those materials have been successfully patterned by photolithography and dry etching techniques. Parallel fabrication of many microbeams was demonstrated. The conducting IPNs have been characterized as microactuators and have demonstrated strain differences up to 0.9% and output forces is the range of µN. Comparison of the experimental output forces with the existing model was performed. Even if the general trend is in accordance with theoretical values, the models developed for classical trilayer actuators reach their limits for such systems which may be due to the non-homogeneous nature of the different layers. Finally, a resonant frequency as high as 930 Hz was observed, revealing that ion movements are still present at such frequencies. These results demonstrates that ionic actuation is possible at a frequency that was thought unreachable for such systems if devices are designed as an ultrathin actuator and open up promising prospects in the development of MEMS requiring actuators with large displacement, high speed and low driving voltages.

4. Experimental Section

Materials: Nitrile butadiene rubber with 44 wt% acrylonitrile content (from Lanxess), dicumyl peroxide (DCP, from Aldrich, 98%), Cyclohexanone (Acros, 99.8%), poly(ethylene glycol) dimethacrylate (PEGDM, Mn = 750 g mol^{-1}, Aldrich), poly(ethylene glycol) methyl ether methacrylate (PEGM, Mn = 475 g mol^{-1}, Aldrich), anhydrous iron III chloride (from Acros), 3,4-ethylenedioxythiophene (EDOT, H.C.Starck) was distilled under reduced pressure, Dicyclohexylperoxidicarbonate (DCPD, Groupe Arnaud). 1-ethyl-3-methylimidazolium bis-(trifluoromethanesulfonyl)imide (EMITFSI, Solvionic, electrochemical grade 99%), aqueous solution of Polyvinylalcohol 300 g L^{-1} (PVA from Acros, Mw = 2000 g mol^{-1}).

Poly(ethylene oxide)/Nitrile butadiene Rubber Thin Film Synthesis: PEO/NBR 50/50 IPN films are obtained by an in-situ polymerization according to a modified method of previously described procedure.[26] First the linear NBR solution is prepared by dissolving NBR in cyclohexanone (1:5 weight ratio). After complete dissolution, DCP (6 wt% vs NBR) as crosslinker was then added to the mixture. PEO network precursors (50 wt% vs NBR) are introduced by adding PEGM monomer (75 wt% of the PEO network) and PEGDM crosslinker (25 wt% of the PEO network). DCPD initiator (3 wt% PEO precursors) was then introduced and the mixture was stirred for 30 min under vacuum. When homogenization was achieved, aqueous PVA solution at 300 g L^{-1} was firstly spincoated onto a glass slide (3000 rpm, 3000 rpm s^{-1} for 30 s, corresponding to 2.2 µm thick layer) and dried at 80 °C. Afterwards, the homogeneous mixture of PEO and NBR was spincoated. The thickness of the polymer films depends on the selected spinner speed, time and solution viscosity. The substrate is then kept at 50 °C for 4 h and then postcured for 2 h at 80 °C. The temperature is then increased for 60 min at 160 °C for the crosslinking step of NBR. The lift-off of the PEO/NBR IPN is carried out in water by dissolving the PVA sacrificial layer. The resulting PEO/NBR IPNs were then dried 4 h at 70 °C under vacuum. Freestanding PEO/NBR IPNs are thus obtained.

Trilayer Actuators Preparation: The methodology for the preparation of conducting IPN actuators has been described previously.[30] IPN films are swollen with EDOT vapor under reduced pressure for given lengths of time. The swollen films were then immersed in an iron III trichloride $FeCl_3$ aqueous oxidative solution (1.5 mol L^{-1}) for an oxidative polymerization of EDOT. This synthetic pathway ensures a non-homogeneous distribution of the electronic conducting polymer throughout the thickness of the PEO/NBR IPN. After polymerization, the resulting films were washed with methanol, that is, excess of $FeCl_3$ is removed, and dried under vacuum at 40 °C for 1 h. The edges of the thin film were then trimmed off. The chemical synthesis was optimized to avoid as much as possible short circuit between the two ECP electrodes. Very thin C-IPN films of 3.5 to 14 µm are obtained. Prior to electrochemomechanical characterization, the actuators were immersed in EMITFSI for at least 72 h until saturation.

Microactuators Patterning Process: Patterning using standard photolithography and a dry etching technique were carried out according to a procedure described elsewhere.[11] Firstly, C-IPN films were fixed on silicon substrates with a PVA adhesive layer (from a spincoated aqueous solution at 1500 rpm/750 rpm s^{-1} for 15 s, 5 µm thick layer was obtained). The positive photoresist SPR220–7 µm (Microchem Corporation) is spincoated at 1000 rpm for 40 s, with a ramp rate of 750 rpm s^{-1}. The softbake for SPR220 was 115 °C on a contact hotplate with slow ramp up and down to avoid formation of cracks. The resulting ≈17 µm thick photoresist is then patterned. Photoresist was exposed through a mask to an energy dose of 400 mJ cm^{-2} during 40 s with a light at 365 nm. A hold time of at least 180 min is required to complete the photoreaction before the next step.[34] The sample is then soaked in the corresponding photoresist developer (Microchem Corporation MF-326) for 10 min in order to obtain a patterned protective layer on top of the C-IPN. In a second step, dry etching of C-IPN was achieved using reactive ion etching. The C-IPN actuators were etched with a mixture of O_2/CF_4 gas (90/10) at 300 W and 200 mT. Finally, the remaining photoresist is removed with acetone and the C-IPN lift-off was carried out by dissolution of PVA sacrificial layer in water. Ionic liquid incorporation was then performed producing self-standing microactuators.

Dynamic Mechanical Thermal Analysis (DMTA): DMTA measurements were carried out on thick film samples with a Q800 apparatus (TA Instruments) operating in tension mode. Experiments were performed at a 1 Hz frequency and a heating rate of 3 °C min^{-1} from –90 °C to 160 °C. Typical dimensions of the samples were 15 mm × 8 mm × 0.25 mm. The setup provides the storage and loss moduli respectively E' and E'', and the damping parameter or loss factor, tanδ.

Mechanical Strength: Mechanical elongations were measured by a mechanical testing machine UNIMAT plus 050–2 kN (ERICHSEN). Samples were cut in strips (Typical dimensions of the samples were 15 mm × 8 mm × 0.25 mm.) The strips were fixed between two clamps, dawn by a constant velocity (20 cm min^{-1}) at room temperature, and stress versus strain curves were recorded.

Swelling Ratio: The swelling ratio was determined by weighting the samples before and after EDOT gas phase swelling and calculated with the following relationship:

$$\text{Swelling ratio (\%)} = \frac{w_s - w_o}{w_o} \times 100 \quad (6)$$

with w_0 and w_s the mass of the sample before and after the swelling step.

Ionic and Electronic Conductivity Measurements: The ionic conductivity was measured by means of impedance spectroscopy using a VSP potentiostat (BiologicSA). The experiments were performed in a temperature range from 20 °C to 100 °C by steps of 10 °C, in the frequency range of 0.01–100 MHz, with a rate of 6 points per decade and for an oscillation potential of 10 mV. PEO/NBR IPN, permeated with electrolyte, was fixed in a cell with pressure contact stainless steel electrodes. The ionic conductivity σ_i is calculated using the equation:

$$\sigma_i = \frac{h}{Z \times S} \quad (7)$$

where Z is the real part of the complex impedance, h is the thickness of the sample, and S is the sample area. The effective electronic conductivity of electrochemical ECP layers in dry state was estimated with home-made 4-point probe, according to Smits equation:[35]

$$\sigma_e = I \times (4.532 \times h_1 \times V)^{-1} \quad (8)$$

where σ_e is the effective electrical conductivity, h_1 is the total thickness of the interpenetrated PEDOT electrode, I is the applied constant current between outer contacts of probe, and V is the measured voltage between inner-contacts.

Scanning Electron Microscopy and Energy Dispersive X-Ray Spectroscopy: Scanning electron microscopy (SEM) was performed using a Carl Zeiss AG-ULTRA 55 by GEMINI with a field emission gun at 2–10 kV. The SEM is equipped with an energy dispersion spectrometer (EDS) allowing a sulfur mapping on the conducting IPN (HV = 10 kV).

Electrochemomechanical Characterizations: The frequency-dependent tip displacements of the microactuators were measured using a laser displacement sensor (Keyence laser LK-G32). From the resulting displacement signal, strain difference between the electrodes was calculated according to Sugino et al.:[36]

$$\varepsilon = \frac{2 \times D \times h}{L^2 + D^2} \quad (9)$$

where ε is the strain difference, D is half of the peak to peak displacement, h is the thickness of the actuator (measured with SEM microscope after swelling in electrolyte), and L is the distance from the clamped end of the actuator to the projection of the laser. The output force was measured using a FT-S Microforce Sensing Probes from FemtoTools. Microforce sensors are capable of measuring forces from millinewtons (10^{-3} N) down to several nanonewtons (10^{-9} N) along the sensors' probe axis. Both compression and tension forces can be measured. The measured force is calculated by the equation F = Sensor Gain × ($V_{out} - V_{out,0}$), where F is the force axially applied to the sensor

probe, $V_{out,0}$ is the output voltage at zero load, and V_{out} is the output voltage as the load is applied. A tensile force will result in an increase of the output voltage whereas a compression force will result in a decrease of the output voltage. Each individual sensor is delivered with calibration data sheet.

Supporting Information

Supporting Information is available from the Wiley Online Library. Experimental data about thickness of the PEO/NBR IPN as a function of spin speed, experimental details and results about determination of the stiffness and output force of the microbeam. Additional SEM images.

Acknowledgements

The authors would like to thanks the ANR for its financial support (Grant No. ANR-09-BLAN-0110) and the European Network on Artificial Muscles (ESNAM).

Received: February 3, 2014
Revised: March 10, 2014
Published online: May 12, 2014

[1] R. H. Baughman, *Synth. Met.* **1996**, *78*, 339.
[2] E. Smela, *Adv. Mater.* **2003**, *15*, 481.
[3] T. Mirfakhrai, J. D. W. Madden, R. H. Baughman, *Mater. Today* **2007**, *10*, 30.
[4] S. A. Wilson, R. P. J. Jourdain, Q. Zhang, R. A. Dorey, C. R. Bowen, M. Willander, Q. U. Wahab, S. M. Al-hilli, O. Nur, E. Quandt, C. Johansson, E. Pagounis, M. Kohl, J. Matovic, B. Samel, W. van der Wijngaart, E. W. H. Jager, D. Carlsson, Z. Djinovic, M. Wegener, C. Moldovan, R. Iosub, E. Abad, M. Wendlandt, C. Rusu, K. Persson, *Mater. Sci. Eng. R Rep.* **2007**, *56*, 1.
[5] E. W. Jager, O. Inganäs, I. Lundström, *Science* **2000**, *288*, 2335.
[6] Y. Fang, X. Tan, *Sensors Actuators A Phys.* **2010**, *158*, 121.
[7] E. W. H. Jager, E. Smela, O. Inganas, I. Lundstrom, *Synth. Met.* **1999**, *102*, 1309.
[8] E. Smela, *J. Micromech. Microeng.* **1999**, *9*, 1–18.
[9] T. F. Otero, M. T. Cortés, *Sensors Actuators B Chem.* **2003**, *96*, 152.
[10] G. Alici, V. Devaud, P. Renaud, G. Spinks, *J. Micromech. Microeng.* **2009**, *19*, 025017.
[11] A. Khaldi, C. Plesse, C. Soyer, E. Cattan, F. Vidal, C. Legrand, D. Teyssié, *Appl. Phys. Lett.* **2011**, *98*, 164101.
[12] Y. Wu, G. Alici, G. M. Spinks, G. G. Wallace, *Synth. Met.* **2006**, *156*, 1017.
[13] B. Gaihre, G. Alici, G. M. Spinks, J. M. Cairney, *Sensors Actuators A Phys.* **2011**, *165*, 321.
[14] L. H. Sperling, In *Interpenetrating Polymer Networks*, American Chemical Society, USA **1994**, pp 3–38.
[15] A. Khaldi, C. Plesse, C. Soyer, C. Chevrot, D. Teyssié, F. Vidal, E. Cattan, In *Proceedings of SPIE The International Society for Optical Engineering*, Vol. *1* (Ed: Y. Bar-Cohen) **2012**, pp.83400J–83400J–9.
[16] C. Plesse, F. Vidal, C. Gauthier, J.-M. Pelletier, C. Chevrot, D. Teyssié, *Polymer* **2007**, *48*, 696.
[17] L. J. Goujon, A. Khaldi, A. Maziz, G. T. M. Nguyen, P. Aubert, C. Chevrot, D. Teyssie, *Macromolecules* **2011**, *44*, 9683.
[18] N. Festin, C. Plesse, P. Pirim, C. Chevrot, F. Vidal, *Sensors Actuators B Chem.* **2014**, *193*, 82.
[19] E. Marwanta, T. Mizumo, N. Nakamura, H. Ohno, *Polymer* **2005**, *46*, 3795.
[20] M. S. Cho, H. J. Seo, J. D. Nam, H. Choi, J. C. Koo, K. G. Song, Y. Lee, *Sensors Actuators B Chem.* **2006**, *119*, 621.
[21] K. I. Kim, S. C. Kim, *Polym. Bull.* **1992**, *29*, 393.
[22] H. Q. Xie, Z. H. Liu, H. Liu, J. S. Guo, *Polymer* **1998**, *39*, 2393.
[23] Z. Cai, J. Kim, *J. Appl. Polym. Sci.* **2008**, *109*, 3689.
[24] S. Machida, S. Miyata, A. Techagumpuch, *Synth. Met.* **1989**, *31*, 311.
[25] E. Smela, *MRS Bull.* **2011**, *33*, 197.
[26] N. Festin, A. Maziz, C. Plesse, D. Teyssié, C. Chevrot, F. Vidal, *Smart Mater. Struct.* **2013**, *22*, 104005.
[27] G. Alici, N. N. Huynh, *Sensors Actuators A Phys.* **2006**, *132*, 616.
[28] P. Madden, Development and modeling of conducting polymer actuators and the fabrication of a conducting polymer based feedback loop, PhD thesis, Massachusetts Institute of Technology **2003**.
[29] R. D. Blevin, *Formulas for natural frequency and mode shape*, Van Nostra, New York, USA **1978**, p.108.
[30] C. Plesse, A. Khaldi, Q. Wang, E. Cattan, D. Teyssié, C. Chevrot, F. Vidal, *Smart Mater. Struct.* **2011**, *20*, 124002.
[31] J. D. Madden, R. A. Cush, T. S. Kanigan, I. W. Hunter, *Synth. Met.* **2000**, *113*, 185.
[32] T. F. Otero, *Handbook of Organic and Conductive Molecules and Polymers* (Ed: H. S. Nalwa) J. Wiley & Sons, Chichester, UK **1997**, p. 517.
[33] G. Klaasse, R. Puers, H. Tilmans, In *Proceedings 3rd Workshop on Semiconductor Sensor and Actuator* **2002**, pp.631–634.
[34] C. Koch, T. J. Rinke in Application Note on Lithography: Theory and Application of Photoresists, Developers, Solvents and Etchants, Microchemicals GmbH, Ulm, Germany **2008**.
[35] F. M. Smits, *Bell Syst. Tech.* **1958**, *37*, 711.
[36] T. Sugino, K. Kiyohara, I. Takeuchi, K. Mukai, K. Asaka, *Sensors Actuators B Chem.* **2009**, *141*, 179.